Optically Directed Assembly of Continuous Mesoscale Filaments

J. T. Bahns, S. K. R. S. Sankaranarayanan, S. K. Gray, and L. Chen

Phys. Rev. Lett. **106**, 095501 — Published 28 February 2011

DOI: 10.1103/PhysRevLett.106.095501

Optically Directed Assembly of Continuous Mesoscale Filaments

J. T. Bahns[1], S.K.R.S. Sankaranarayanan[2], S. K. Gray[2], L. Chen[1]*
[1]Biosciences Division, [2]Center for Nanoscale Materials,
Argonne National Laboratory, Argonne, IL 60439

ABSTRACT

We demonstrate irreversible continuous filament formation when a weak laser focus is positioned near the edge of an evaporating colloidal droplet containing carbon and gold nanoparticles. Optical trapping, hydrothermal and chemical interactions lead to controlled colloidal synthesis of stable, irreversible mesoscale filaments of arbitrary shape and size. Mechanisms for this optically directed assembly are discussed with fluid dynamics, molecular dynamics, and lattice kinetic Monte-Carlo calculations.

PACS numbers: 81.16.Mk, 82.70.Dd, 62.23.st, 47.11.j, 47.11.Fj, 47.11.Mn

Synthesis of hierarchical materials with controlled shapes and sizes relies on manipulating matter from the atomic to microscale [1]. Colloidal nanoparticles (NPs) are convenient building blocks for such materials [2]. For example, after a colloidal NP droplet is placed on a surface, NPs are transported from the bulk toward its edge by convective forces, causing increased particle densities near the edge, ultimately forming a "coffee-ring" stain [3, 4]. This effect has been used to generate various ordered self-assembled structures [5].

However, controlled synthesis of "user-designed" architectures from colloidal NPs that extend over microscopic and mesoscopic length scales is challenging due to a lack of understanding of the growth mechanisms and parameters defining the final architecture [6]. Other challenges are the stability of the assembled NPs and the fact that surfactant layers might limit the durability of mesoscopic aggregations. Controlled irreversible assembly of stable NP structures with intricate shapes and arbitrary sizes requires fine-tuning the balance of numerous forces that drive the assembly [6].

Laser-induced aggregation of noble metal NPs has been the subject of numerous studies. At low irradiation intensities (e.g. lamps, unfocused lasers), NP aggregation occurs only after hours of irradiation [7-9]. Visible irradiation near the Mie resonance is more efficient at producing aggregates [10-13] (minutes). Higher intensities ($> 10^6$ W/cm^2) are required for aggregation on shorter time scales [14, 15]. In these studies, aggregate shapes cannot be controlled, resulting in scattered NP clusters, doughnut-shaped micro-structures, etc., and special colloid treatments (e.g. various capping strategies) are needed to enhance aggregation and mitigate dissociation.

In this Letter, we demonstrate optically directed assembly (ODA), which allows formation of stable nanoscale and mesoscale structures with arbitrary shapes through an optically directed and hydrothermally controlled process. The mesoscale structures do not require the presence of a capping layer. Furthermore, ODA occurs at low power and on millisecond timescales.

Using a colloidal droplet containing carbon and gold NPs, we find that when a weak (~1 mW/ 0.3 μm^2) optical trap is positioned within ~30 μm of the droplet edge, continuous ODA of the mixed NPs occurs at the laser focus. In particular, because the NPs bind irreversibly in the trap a striking new aggregation outcome results: The tiny (femto-liter) laser trap becomes a mobile nucleation site, capable of spatially directing aggregation, forcing it to occur wherever the trap is moved. We demonstrate two ODA modes (Fig. 1, supporting online materials Figs. S1, S2, and videos V1-V3 [16]): (1) A steady-state mode occurs when the trap is stationary above the glass surface. A long, thin, continuous filament grows out of the trap top and extends vertically towards the air-droplet interface (Figs. 1(a), (d), (e), (f)); (2) A drawing/welding mode occurs when the trap is moved to a solid surface or positioned onto an existing filament, with additional NPs accumulating irreversibly wherever the spot is located, enabling “drawing” of simple shapes and "welding" to make more complex assemblies (Figs. 1(b), (c), video V2 [16]). Supporting calculations help explain why ODA has been experimentally observed thus far only in a narrow annular domain near the edge of an evaporating colloid droplet, whereas not in a droplet interior or in a large sealed cell designed to mimic the bulk equilibrium [16].

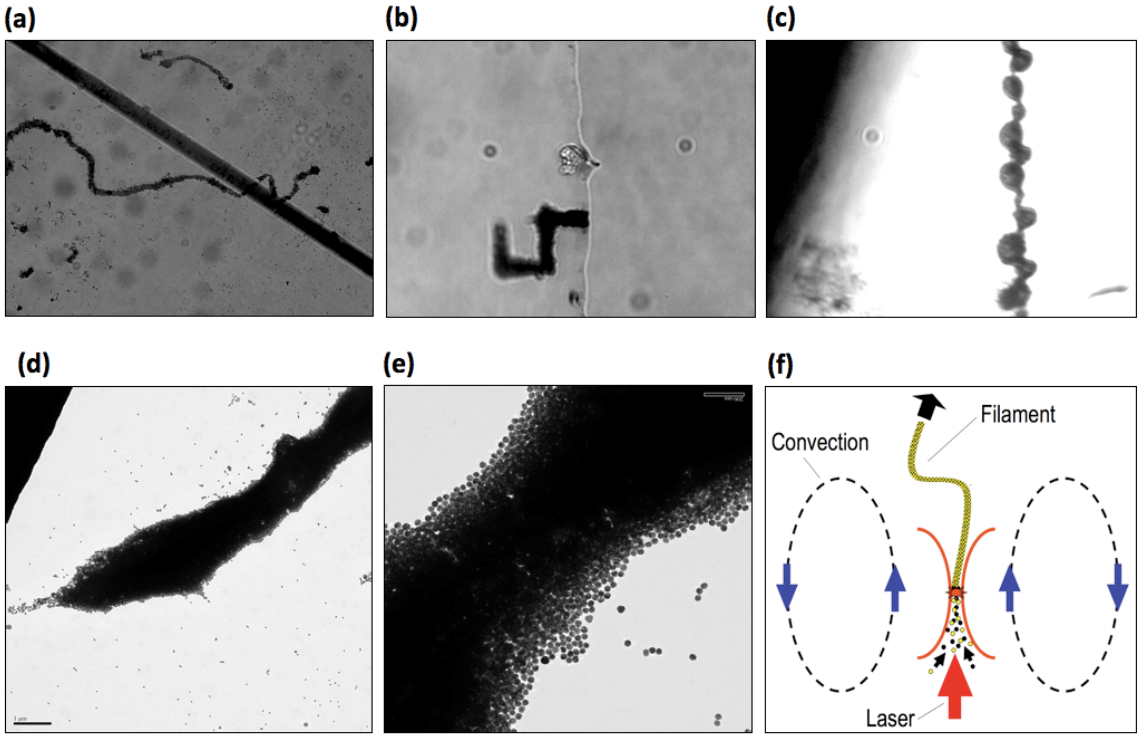

FIG. 1 (color online). ODA of mesoscale structures. (a) Optical image of a gold/carbon filament obtained with a stationary optical trap. The thick black feature is a 7 μm diameter carbon fiber. (b) Hook-shaped gold/carbon structure form by slow translation of the trap. (c) Lobe-shaped filament form by translating the trap with varying speeds. Slower speeds cause larger filament diameters and vice versa. (d) TEM image of a filament grown on a TEM grid. The sharp tip is caused when the filament stops growing due to local colloid depletion. (e) Close-up of (d) showing a dense "neck". This illustrates how filament radial dimensions are influenced by the radial component of the trap potential. (f) Schematic ODA model: NPs drawn into the optical trap from below by convection irreversibly bind at the focus.

To further understand filament growth during steady-state ODA, we monitor the temporal behavior of the transmitted trap laser light under sub-threshold (low power) filament growth conditions (Fig. 2). Trap loading, preceding continuous filament growth,

arises from two features: (i) particle diffusion into the trap and fusing (region I) and (ii) formation of a hydrothermal jet coincident with the optical trap that invokes convective (toroidal) loading which increases filament growth rate (region II). Immediately following region II, the transmitted intensity increases abruptly due to the filament falling out of the trap, and the process repeats.

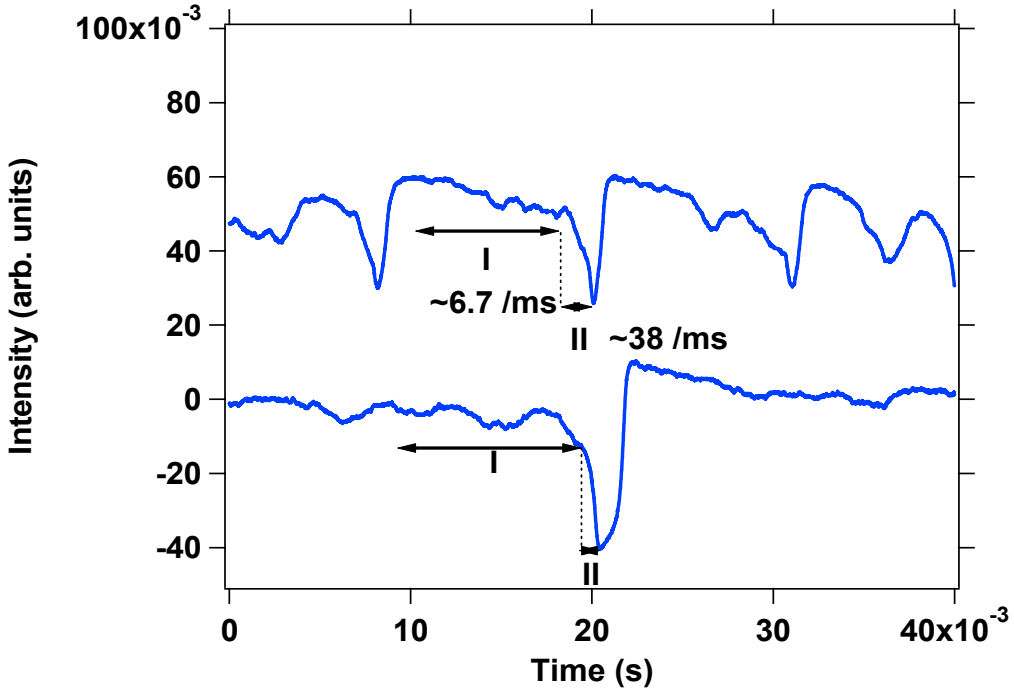

FIG. 2. Sub-threshold filament growth in the steady-state ODA mode (stationary trap). Two vertically displaced traces of transmitted laser light illustrate the characteristic slow attenuation region (I), corresponding to diffusional trap loading, followed by an enhanced attenuation region (II) due to the faster hydrothermal loading.

The hydrothermal character of ODA is further elucidated by computational fluid dynamics (CFD) simulations of the Navier-Stokes and heat transfer equations that model fluid flow and temperature variation due to laser irradiation [16]. We treat the trap as a source of energy that induces hydrothermal convection within the droplet. Fig. 3(a) shows the fluid velocity vectors at steady state that result when a (fixed) 500 nm carbon

NP, located both near the glass surface and droplet edge, is at the center of the laser focus. These results are indeed consistent with toroidal circulation with fluid velocities up to 300 μm/s (Table S1 [16]). Such a fluid flow can result in enhanced particle densities within the optical trap. The corresponding temperature distribution (Fig. 3(b)) indicates significant heating near the laser focus above ambient temperature (300 K), with maximum increase ~30 K (with 1.5 mW power). The contours in Fig. 3(b) show that the highest temperatures occur near the NP surface. The fluid flow resulting from this heating is driven by buoyancy due to changes in fluid density with temperature. This change in density when acted upon by gravity causes upward movement of the lighter fluid (as with candle flames) while the heavier fluid flows downward (towards gravity). This sets up a toroidal convection current (Fig. 3(a)).

If one considers carbon NPs further away from the glass surface, but still near the droplet edge, comparable flow patterns and temperature increases result (Fig. S4). However, the fluid velocities are an order of magnitude higher (Table S1), implying increased convective loading. Experimentally it is also much easier to form filaments when the laser focus is near the droplet surface but somewhat removed from the glass surface.

We carried out similar calculations for gold NPs (Table S2). While the wavelengths considered here are somewhat removed from the surface plasmon resonance, the NP optical response is still sufficiently strong to generate a ~10 fold local intensity enhancement near particle surfaces. Accounting for this leads to comparable flow patterns, but somewhat higher temperature increases ~ 60-120K.

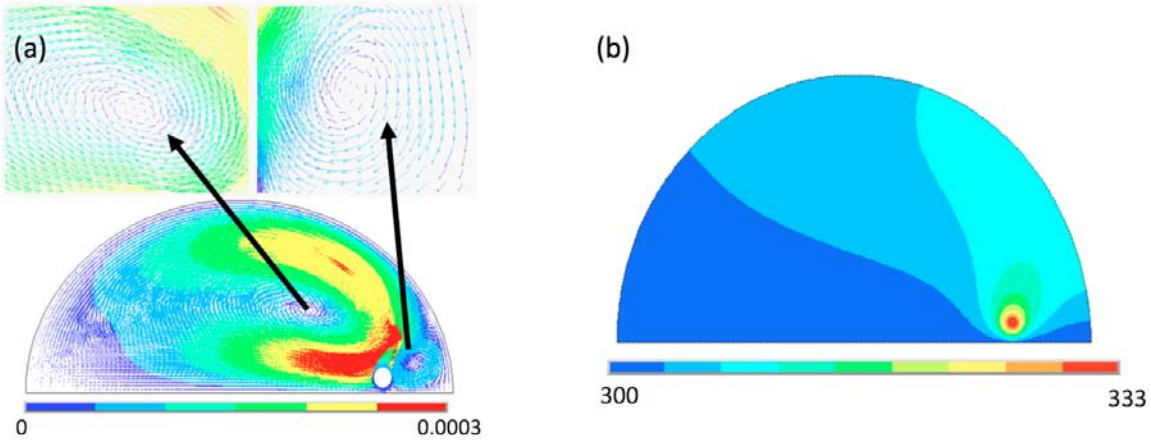

FIG. 3 (color online). CFD results for laser heating of a carbon NP. The droplet radius is 1300 μm. (a) 2-D steady-state fluid vector plots from heating a carbon NP (filled white circle) located on the glass surface, with a focused 1.5 mW laser (units: m/s). Vortices form by the toroidal circulation. The velocity vectors rotate anti-clockwise in the left blow-up and clockwise in the right blow-up, consistent with funneling just above the NP between these regions. (b) Resulting temperature profiles (units: K). A hydrothermal jet can be seen extending vertically above the particle.

Atomic-level dynamics is also an essential aspect of ODA. Electron microscopy images (Fig. 4(a) and (b)), reveal an amorphous structure, suggesting a predominance of carbon-to-carbon and carbon-to-metal close-packing between NPs. Irreversible metal-to-metal aggregating is observed only when carbon is present. Limited carbon-to-carbon coalescence is observed in the absence of gold, but no continuous filament growth results when either pure metal or carbon solutions are used, suggesting a cooperative effect between dissimilar particles. We outline two possible microscopic scenarios consistent with the observations.

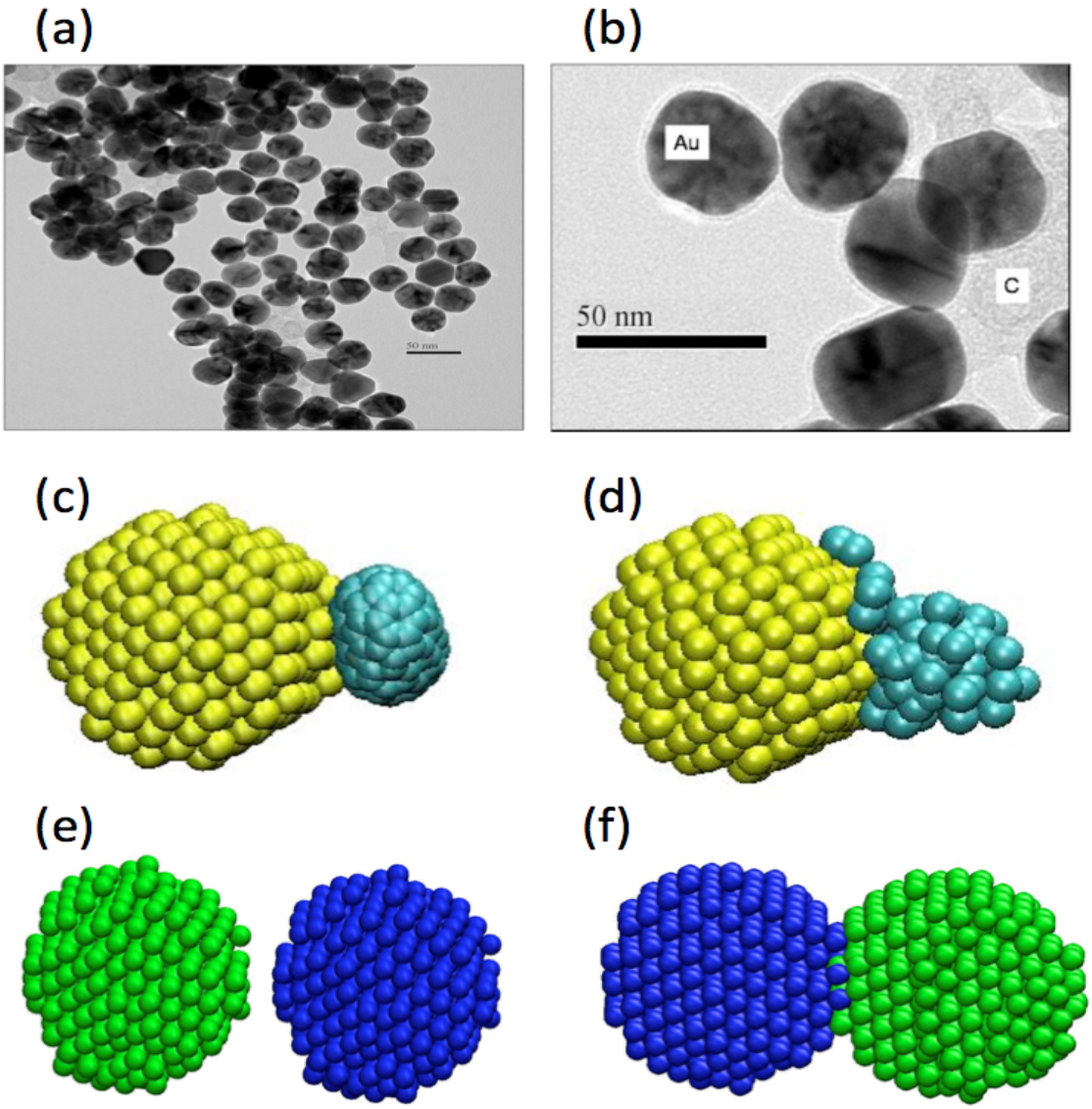

FIG. 4 (color online). Gold/carbon NP interactions. (a) TEM image of the extreme tip of the gold/carbon filament in Fig. 1(d). (b) TEM image of encapsulated gold NPs within the tip. (c) Initial gold/carbon NP configuration for a MD simulation. (d) MD result after 10 ns showing wetting of a gold NP by carbon atoms in the 450 K range. These results indicate the possibility of encapsulation of gold NPs by carbon. (e) Initial configuration of gold-gold interaction for the MD simulation. (f) Snapshot showing result after 10 ns at 500 K.

Examination of TEM images (Figs. 4(a), (b)) reveals enhanced encapsulation of gold NPs by an opaque material, presumably carbon. Carbon encapsulation of the gold

NPs may therefore play a key role. In our first microscopic scenario, we hypothesize that localized heating, coupled with hydrodynamic forces are sufficient to detach ligands from the metal particles. At the elevated temperatures predicted by the CFD simulations, carbon NPs may "wet" the gold NPs, leading to carbon-encapsulated gold NPs that subsequently can bind with one another. However, the temperature rise is not sufficient to induce gold-gold coalescence. We carried out molecular dynamics (MD) simulations to support this picture (Figs. 4(c), (d)). These figures show that carbon atoms have a tendency to wet the gold surface at 450 K. (The process initiates at a lower temperature of 400 K.) Such coalescence does not happen in gold-gold NP interactions (Figs. 4(e),4(f)). (Gold coalescence only occurs at temperatures above 600-700 K, which are not reached with the laser powers of this study.)

The gold NPs are covered by citrate surfactant ligands that stabilize the colloid. The scenario above assumes these ligands are readily displaced and play no role. While citrate binding to gold nanoparticles is relatively weak [17], it is still possible that citrate might be involved in the binding process. A second microscopic scenario is that the ligands are not removed from the nanoparticle surface. In this case, carbon prefers to wet or react with the citrate ligand and the presence of the ligands prevents gold-gold NP coalescence.

To further validate the ODA mechanism, we use a multi-scale model combining the continuum CFD results with a lattice kinetic Monte Carlo (LKMC) approach to model the growth kinetics and filament assembly [18]. These simulations also allow for the initial non-equilibrium conditions resulting from evaporation-induced transport. See [16] for more detail. The LKMC model accounts for particle-particle interactions via

coalescence efficiencies. Consistent with either microscopic scenario above, the coalescence efficiency for gold-gold is taken to be two orders of magnitude smaller than of carbon-carbon. This efficiency range is typical of those in other colloid simulations [19]. Deposition assembly rates obtained for varying gold NP fraction are compared with experimental results (Fig. 5).

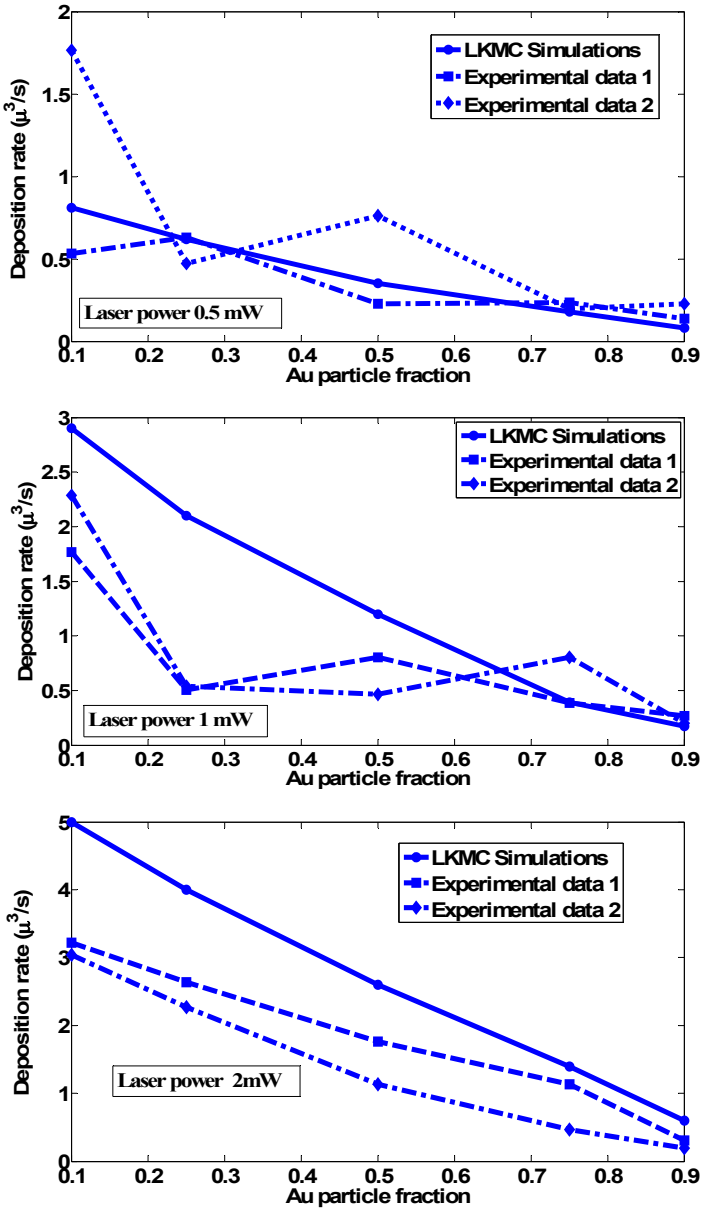

FIG. 5 (color online). LKMC and experimental deposition for laser powers 0.5 (top), 1 (middle) and 2 mW (bottom). Two different experimental data sets are displayed for mixed colloids (all at fixed gold NP concentration 7.2×10^{10} cm^{-3}).

Given the simplicity of the model, the agreement between experimental and calculated filament deposition rates is remarkably good (Fig. 5). One sees that the growth kinetics increases significantly as gold fraction is varied from 90% to 10%. The convection frequencies are dictated by the location of the particle in the LKMC lattice and are higher near the optical trap where particle velocities are highest (Fig. 3). Hence, the probability of nucleation of the filament is most likely at the optical trap. For given colloidal composition, increased laser power results in increased convection velocities and higher deposition rates. For given laser power, as the gold fraction decreases, the gold-carbon and carbon-carbon collision frequencies become significant. This leads to increased gold-carbon wetting and higher filament growth rates at lower gold fractions. The net growth rate is dictated by the relative frequencies of coalescence and convection. Tuning these interactions at the nanoscale is key to controlling the dynamics of formation of structures from the nanoscale to mesoscale.

Our measurements and calculations indicate that ODA takes place via cohesive laser trapping, hydrothermal and chemical effects. This picture accounts for the hydrothermal (toroidal) circulation that "funnels-in" colloidal NPs below the trap for optically directed assembly into a solid, close-packed filament. The resulting filament structures could be excellent candidates for various applications. For example, in the Supporting Online Material we demonstrate surface enhanced Raman spectroscopy with the filament structures [16, 20]. ODA also works with the combination of silver and

carbon NPs, suggesting that binary colloids of other elements might also be optically assembled. To better understand ODA, many fundamental questions remain such as the role played by ligands, the exact nature of the binding mechanism holding the filaments together, and the assembly of other binary NP combinations.

JTB and LC acknowledge the U. S. Department of Energy, Office of Science, Office of Biological and Environmental Research, under grant no. BER-6132800. Use of the Center for Nanoscale Materials was supported by the U. S. Department of Energy, Office of Science, Office of Basic Energy Sciences, under Contract No. DE-AC02-06CH11357. We thank the University of Southern Florida for providing computational facilities, Yi Mei and Q. Guo for providing images, N. F. Scherer and the anonymous reviewers for helpful comments.

*jbahns@anl.gov

References

[1] Y. Xia, B. Gates, Y. Yin, and Y. Lu, Adv. Mater. **12**, 693 (2000).

[2] R. D. Deegan *et al.*, Nature **389**, 827 (1997).

[3] T. P. Bigioni *et al.*, Nature Mater. **51**, 265 (2006).

[4] S. T. Chang, and O. D. Velev, Langmuir **22**, 1459 (2006).

[5] B. G. Prevo, D. M. Kuncicky, and O. D. Velev, Colloids and Surfaces A **311**, 2 (2007).

[6] Z. Mao, H. Xu, and D. Wang, Adv. Funct. Mater. **20**, 1053 (2010).

[7] H. Hasegawa *et al*., Z. Phys. D **20**, 325 (1991).

[8] N. Satoh *et al*., J. Phys. Chem. **98**, 2143 (1994).

[9] J. Zhou *et al*., Langmuir **24**, 4506 (2008).

[10] H. Eckstein, and U. Kreibig, Z. Phys. D **26**, 239 (1993).

[11] N. Harris *et al*., Nanotechnol. **18**, 365301 (2007).

[12] Y. Takauchi, T. Ida, and K. Kimura, J. Phys. Chem. B **101**, 1322 (1997).

[13] Y. Zhang *et al*., Phys. Rev. B **9**, 165405 (2006).

[14] Y. Tanaka *et al*., Opt. Exp. **17**, 18760 (2009).

[15] H. Yoshikawa, T. Matsui, and H. Masuhara, Phys. Rev. E **70**, 061406 (2004).

[16] See EPAPS document No. [ ] for details and ODA videos V1-V3.

[17] B. D. Chithrani, A. A. Ghazani, and W. C. W. Chan, Nano Lett. **6**, 662 (2006).

[18] D. Frenkel, B. Smit, *Understanding Molecular Simulation: From Algorithms to Applications.* (Academic Press, New York, 1996).

[19] R. Bandyopadhyaya, R. Kumar, and K. S. Gandhi, Langmuir **16**, 7139 (2000).

[20] J. T. Bahns *et al*., J. Phys. Chem. C **113**, 11190 (2009).